Aerodynamic Effects of Distributed Spanwise Blowing on a Fighter Configuration

Jarrett K. Huffman* and David E. Hahne†
NASA Langley Research Center, Hampton, Virginia
and
Thomas D. Johnson Jr.‡
PRC Kentron, Inc., Hampton, Virginia

A series of low-speed wind-tunnel tests were performed in the NASA Langley 7- by 10-Foot High-Speed Tunnel and 30- by 60-Foot Tunnel to investigate the effects of distributed spanwise blowing. Static longitudinal data were obtained for a range of outer panel nozzle sweep and elevation angles, blowing distributions, leading- and trailing-edge flap deflections, and blowing coefficients up to 24-deg angle of attack. Lateral-directional stability data were obtained to 45-deg angle of attack. Using realistic blowing rates, the ensuing jet flow stabilized the leading-edge vortices and produced significant lift increments at higher angles of attack. Distributing the spanwise blowing improved the lift with larger increases occurring as the blowing was shifted from the inboard to the outboard nozzles; however, this had detrimental effects on the longitudinal- and lateral-directional stability characteristics. Leading-edge flaps delayed the favorable lift effects of spanwise blowing but improved the longitudinal- and lateral-directional stability characteristics. Blowing improved the lift effectiveness of trailing-edge flaps. Tethered free-flight tests showed that spanwise blowing delayed directional divergence to higher angles of attack and alleviated wing rock by providing increased roll damping.

Nomenclature

a.c. = aerodynamic center
A_e = nozzle exit area, in^2
AF = axial force, lbf
b = wing span, ft
$c,\bar{c}$ = local wing and mean aerodynamic chords, respectively, ft
C_L = lift coefficient, lift/$q_\infty S_{\text{ref}}$
C_ℓ = rolling moment coefficient, $M_X/q_\infty S_{\text{ref}} b$
C_{ℓ_p} = $\partial C_\ell/\partial(pb/2V)$
C_{ℓ_β} = $\partial C_\ell/\partial\beta$
$C_{\ell_{\dot\beta}}$ = $\partial C_\ell/\partial(\dot\beta b/2V)$
C_m = pitching moment coefficient, $M_Y/q_\infty S_{\text{ref}}\bar{c}$
C_n = yawing moment coefficient, $M_Z/q_\infty S_{\text{ref}} b$
C_{n_β} = $\partial C_n/\partial\beta$
$C_{n_{\beta,\text{dyn}}}$ = directional divergence parameter, $C_{n_\beta}\cos\alpha-(I_Z/I_X)C_{\ell_\beta}\sin\alpha$
C_T = blowing thrust coefficient, $\sqrt{NF^2+AF^2+SF^2}/q_\infty S_{\text{ref}}$
C_μ = blowing coefficient, $\dot{m}V_j/g_c q_\infty S_{\text{ref}}$
g_c = dimensional constant, 32.17 lbm-ft/lbf-s^2
IB = inboard
I_X,I_Z = mass moments of inertia about longitudinal and normal body axes, respectively, lbm-ft^2
LE = leading edge
$\dot{m}$ = blowing mass flow rate, lbm/s
M_X = rolling moment, ft-lbf
M_Y,M_Z = pitching and yawing moments, respectively, ft-lbf
NF = normal force, lbf
OB = outboard
p = roll rate, rad/s
p_t = plenum stagnation pressure, psia
p_∞ = freestream static pressure, psia
q_∞ = freestream dynamic pressure, psf
R = gas constant, 53.33 ft-lbf/lbm-°R
°R = absolute temperature, deg Rankine
S_{ref} = wing reference area, ft^2
SF = side force, lbf
SWB = spanwise blowing
TE = trailing edge
TOT = total
T_t = plenum stagnation temperature, °R
V = freestream velocity, ft/s
V_j = jet velocity due to isentropic expansion to freestream static pressure, ft/s
W.L. = water line
α = wing angle of attack, deg
β = angle of sideslip, deg
$\dot\beta$ = time rate of change of β, deg/s
ΔC_L = incremental lift coefficient, blowing on C_L − blowing off C_L
θ,Λ_N = outboard nozzle elevation and sweep angles, respectively, deg

Introduction

THE concept of blowing a discrete jet of air spanwise over the upper surface of a wing was extensively studied during the 1970s as a means of improving lift effectiveness.[1-4] When a jet is positioned just aft of and approximately parallel to the leading edges of moderately swept wings, vortices originating from those edges can be enhanced through the mechanism of entrainment and the vortex breakdown phenomenon delayed to higher angles of attack. Thus, the maneuverability of fighter aircraft equipped with spanwise blowing (SWB) can be expected to improve.

Flight verification of this concept was demonstrated in a cooperative program between the McDonnell Aircraft Company and the United States Air Force. The goal was to validate

Presented as Paper 84-2195 at the AIAA 2nd Applied Aerodynamics Conference, Seattle, WA, Aug. 21-23, 1984; received May 13, 1985; revision received April 2, 1986.

*Aero-Space Technologist, NTF Aerodynamics Branch, Transonic Aerodynamics Division. Member AIAA.
†Aero-Space Technologist, Flight Dynamics Branch, Low-Speed Aerodynamics Division. Member AIAA.
‡Project Aeronautical Engineer, Advanced Aircraft Projects. Member AIAA.

wind-tunnel data that showed that the existing chordwise boundary-layer-control (BLC) blowing system in the F-4C/D aircraft could be replaced by a more maintenance-free SWB system without degrading aircraft performance.[5] Though this was a limited program, it did demonstrate that by using engine compressor bleed air to provide SWB at the wing-fuselage juncture (near the leading edges of the wing), the approach speed could be reduced ≈ 7 knots and maneuver performance improved. (The latter was characterized by greater usable angle of attack and load factors, and reduced turn radius.) In addition the handling qualities were improved, i.e., milder wing rock, lower buffet level, and quicker response to control input.

Since the leading-edge jet flow did not penetrate to the outer wing panel, it was suggested that further improvements might result if some of the blowing was distributed over the outer wing panels. Supportive wind-tunnel test results showed that shock-induced separation on a 40-deg swept wing could be reduced with a modest level of outboard blowing.[6] This led to a second wind-tunnel-to-flight research program (the flight research part of this program was canceled) initiated by Dryden Flight Research Facility and Langley Research Center and supported by the United States Air Force. The F-4C aircraft used in the early flight tests was selected as the research vehicle because the prototype SWB system was still in operational status. The Langley contribution, as reported herein, was to conduct wind-tunnel tests to determine 1) the optimum orientation for the outer panel nozzles, 2) how the performance of leading- and trailing-edge flaps and control surfaces are affected by distributed SWB between inboard and outboard nozzles, and 3) the effects of distributed SWB on lateral-directional stability characteristics. Low-speed tests were conducted in the Langley 7- by 10-Foot High-Speed Tunnel and in the 30- by 60-Foot Tunnel to angles of attack of 24 and 45 deg, respectively. Static and dynamic data were acquired for a range of outer panel nozzle parameters, blowing distributions, leading- and trailing-edge flap deflections, and blowing coefficients.

Model and Apparatus

A sketch of the F-4C aircraft is shown in Fig. 1. The appropriate model scale factors are 0.10 for the model tested in the 7- by 20-Foot High-Speed Tunnel and 0.13 for the model tested in the 30- by 60-Foot Tunnel. Photographs of the two models in their respective test sections are shown in Figs. 2 and 3. The models had three segmented leading-edge flaps, trailing-edge flaps, left aileron, right spoiler, all-movable horizontal tail, and conventional rudder. When configured for tethered free-flight tests, the 0.13-scale model incorporated left and right ailerons and spoilers. Deflection angles for the flaps and control surfaces were measured normal to hinge lines and with respect to the plane of the associated surface.

0.10-Scale Model

This model was used in static tests in the 7- by 10-Foot High-Speed Tunnel.[7] High-pressure air used for spanwise blowing was routed from a calibrated venturi through a sting and strain-gage balance to the main plenum in the model. The balance was circular and designed to mount to the air supply pipe, which passed through the center of the balance. The balance eliminated tares associated with high-pressure air as it passed through to the main plenum. Four control valves metered air to the two inboard convergent nozzles and the two outboard convergent nozzle-plenum arrangements. The inboard nozzles were fixed in position at the wing-fuselage juncture and located one nozzle diameter above the wing upper surface and $0.13c$ aft of the wing leading edge. They were aligned parallel to the upper surface and leading edge of the main wing. The variable-angle outboard nozzle arrangements were faired fore and aft and positioned at the wing-fold line ($2y/b = 0.70$) and $0.25c$ aft of the wing leading edge. Since one objective of this research was to optimize SWB on the outer wing panel, the outboard nozzles were designed to have variable sweep (Λ_N) and elevation (θ) angles as shown in Fig. 4. Four sets of nozzles, with $\theta = 9.0$, 12.0, 15.0, and 18.0 deg, were evaluated at $\Lambda_N = 39.1$ to 57.1 deg. Note that θ is measured with respect to the plane of the main wing and that the outer wing panels have 12 deg of dihedral.

0.13-Scale Model

This model was used in static and dynamic captive tests and tethered free-flight tests in the 30- by 60-Foot Tunnel. The static and dynamic force tests were made using an internal strain-gage balance. Compressed air for SWB was brought onboard via a shielded trombone arrangement, which minimized air pressure tares. Reference 8 contains detailed descriptions of the dynamic-force test equipment, setup, and data collection methods.

For the tethered free-flight tests, the model was powered by compressed air brought onboard via a flexible umbilical cord through the top of the model (Fig. 3) and exhausted at the rear. The model was instrumented with two sensor systems: a three-axes rate gyroscope to measure angular rates and a miniaturized boom-mounted $\alpha - \beta$ vane. The flight-control laws, with stability augmentation in all three axes, were programmed into a digital computer that processed sensor data and pilot control inputs to generate signals to drive the pneumatic control-surface actuators on the model. High-pressure air for SWB was also brought onboard through the umbilical cord and was distributed to the nozzles via tee connectors. The inboard nozzles had the same orientation as those on the 0.10-scale model, and the unfaired outboard nozzles were set at $\Lambda_N = 53.6$ and $\theta = 12.0$ deg. While these nozzles were actually of constant diameter, they were scaled to those used on the 0.10-scale model.

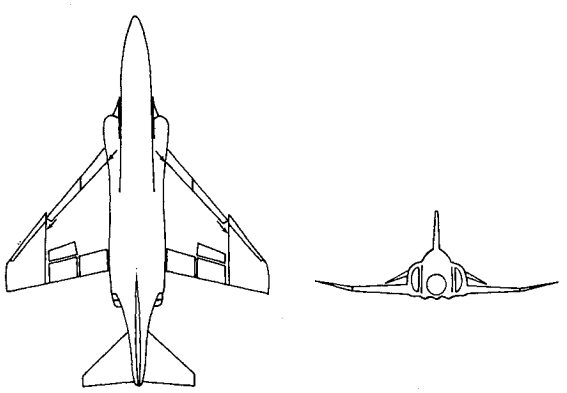

Fig. 1 Sketch of full-scale F-4C aircraft showing relative position of spanwise blowing nozzles.

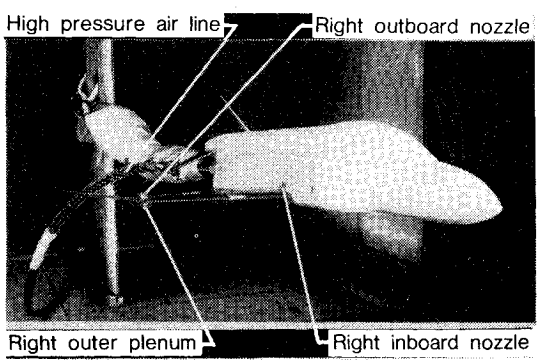

Fig. 2 Photograph of 0.10-scale F-4C model installed in the NASA Langley 7- by 10-Foot High-Speed Tunnel.

Tests and Corrections

7- by 10-Foot High-Speed Tunnel

Static tests were conducted at a Reynolds number of 2.1×10^6 (based on $\bar{c}$) and a Mach number of 0.21. The angle of attack ranged from approximately -1 to 24 deg. Forces and moments were measured by a six-component strain-gage balance, and corrections have been applied to the data. Selected surface flow patterns were photographed using fluorescent oil visualization techniques. Note that the data are untrimmed and that the moments have been referenced to 31% $\bar{c}$ and W.L. 2.66 in., and the horizontal tail was set at the same incidence as the main wing. The thrust effects of SWB have been removed from the data.

Blowing coefficients (C_μ) were varied from 0 up to 0.140. As presently configured, 0.035 corresponds to the maximum available engine bleed air of the test vehicle at full throttle during takeoff and maneuver, while 0.020 is a nominal value for reduced power during landing approach. There were four SWB distributions investigated: blowing with the inboard nozzles only (ALL-IB), 2/3-C_μ inboard and 1/3-C_μ outboard (2/3-IB, 1/3-OB), 1/3-C_μ inboard and 2/3-C_μ outboard (1/3-IB, 2/3-OB), and blowing with outboard nozzles only (ALL-OB).

The total mass flow rate ($\dot{m}_{TOT}$) of the high of high-pressure air used for spanwise blowing was measured by a calibrated venturi upstream of the model, and the plenums were instrumented for total temperature and pressure. The blowing coefficient was determined using the following equations:

$$\dot{m}_{OB} = 0.6847 A_e p_t / \sqrt{RT_t/g_c} \text{ lbm/s}$$

$$\dot{m}_{IB} = \dot{m}_{TOT} - \dot{m}_{OB} \text{ lbm/s}$$

$$V_j = 109.6\sqrt{T_t[1-(p_\infty/p_t)^{2/7}]} \text{ ft/s}$$

$$C_\mu = \dot{m} V_j / g_c q_\infty S_{ref}$$

C_μ was set by controlling the main plenum pressure and temperature using calibration data for the three plenums.

30- by 60-Foot Tunnel

Static and dynamic (forced-oscillation) force tests were conducted at a Reynolds number of 1.23×10^6 based on $\bar{c}$. Static tests were made over an α-range of 0–45 deg and at $\beta = 0$ and ± 5 deg. The forced oscillation tests in roll were conducted between $\alpha = 0$ and 45 deg for $\beta = 0$, with an angular amplitude of ± 5 deg at a frequency of 0.75 Hz. Corrections for flow angularity were applied to the balance data, and the thrust effects of SWB are included in the data.

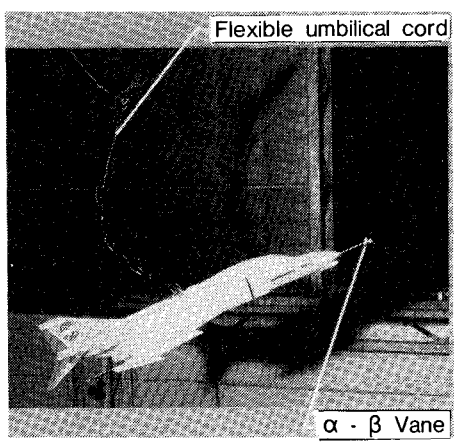

Fig. 3 Photograph of 0.13-scale F-4C model taken during tethered free-flight test in the NASA Langley 30- by 60-Foot Tunnel.

Tethered free-flight tests were flown to determine the dynamic stability and control characteristics with and without spanwise blowing. The model was flown in level flight to high angles of attack, which included studies of wing rock and eventual departure characteristics (i.e., directional divergence or nose slice). The qualitative results of the flight tests consisted of pilots' observations of, and opinions on, the flying qualities of the model and motion pictures made on all flights. Quantitative data consisted of time histories of the model control positions, angular rates, angle of attack, and sideslip angle. See Ref. 9 for a detailed discussion of free-flight test techniques.

Before testing, the left inboard and outboard nozzles were individually calibrated on the model by measuring the balance forces (wind off) and air-line static pressures (just upstream of each nozzle) as the air supply pressure was increased. The resulting forces were resolved into a blowing thrust coefficient

$$(C_T = \sqrt{NF^2 + AF^2 + SF^2}/q_\infty S_{ref})$$

and plotted vs the air-line static pressure. The desired C_T for left and right pairs of nozzles were controlled by setting the corresponding air-line static pressure.

Discussion of Results

The following discussions present results of studies made to determine the near-optimum orientation for the outer panel nozzles, which included effects of sweep (Λ_N) and elevation (θ) angles and variable SWB rates using only outboard blowing. This is followed with discussions of the effects of distributed SWB on the clean and flapped configurations. Longitudinal aerodynamic data, as presented in Figs. 5-10 and 13 and 14, were acquired in the 7- by 10-Foot High-Speed Tunnel and are referenced to the stability axes. Lateral-directional stability data, which are referenced to the body

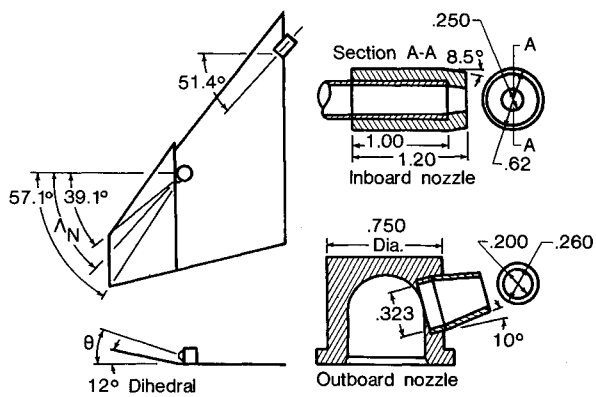

Fig. 4 Sketch and arrangement of nozzles tested on the 0.10-scale F-4C model; 7×10 HST, in.

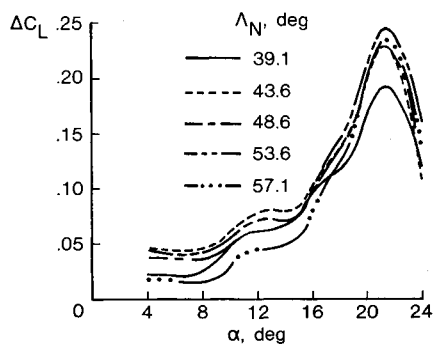

Fig. 5 Effects of outboard nozzle sweep angle on the incremental lift coefficient; clean configuration, ALL-OB, $C_\mu = 0.035$, $\theta = 12.0$ deg.

axes, were acquired in the 30- by 60-Foot Tunnel (Figs. 11, 12, 15, and 16) and include qualitative data in the form of pilot comments.

It should be pointed out that the results of these studies apply to the F-4C configuration and that different results might be obtained on other configurations.

Outer Panel Nozzle Studies

Nozzle Sweep Angle

The effects of Λ_N at constant θ are summarixed in Fig. 5, where the untrimmed incremental lift coefficient data (ΔC_L) are presented for an α-range of 4-24 deg. An oil-flow visualization taken at $\alpha = 6$ deg (Fig. 6a) shows that the flow is attache don the inner wing; however, a vortex has formed on the outer wing panel du to the snag—even on the baseline case ($C_\mu = 0$). Also, the jet is turned chordwise almost immediately after leaving the nozzle and, therefore, it may be concluded that the ΔC_L between $\alpha = 4$ and 8 deg is due to the jet increasing the velocity over a portion of the outer wing panel. The ΔC_L step between $\alpha = 8$ and 12 deg indicates a favorable interaction between the leading-edge vortex and jet. Several things have occurred: as the outer panel vortex grows with α, the low-velocity flowfield associated with the reattachemtn line moves inboard and comes in proximity to the jet, thus enabling the jet to penetrate to the wing tip; and the jet has entrained and stabilized the vortex, thus preventing it from moving further inboard. The plateau in the data between 12 and 15 deg is the consequence of slight changes in the lift slope curves which may be due in part to an increase in effective wing chamber[10] as the jet turns in a more spanwise direction and then becomes fixed in position at $\alpha \approx 12$ deg.

Above $\alpha = 15$ deg, SWB contributes significant lift increments, which are attributed to the ability of SWB to maintain a strong vortex fixed near the leading edge of the outer wing panel while vortex breakdown and wing stall occur on the no-blowing baseline (see Fig. 6b). Note the entrainment of the vortex into the jet. With the exception of $\Delta_N = 39.1$ deg, the data show that nozzle sweep angle is a relatively insensitive parameter at higher α.

Nozzle Elevation Angle

The effects of θ at constant Λ_N are summarized in Fig. 7. The data trends are similar to those just discussed, with the greatest improvement for $\theta = 15.0$ deg. It is apparent that blowing the jet at a 3-deg angle above the outer wing panel allows for more favorable conditions for the jet to expand to ambient conditions. This hypothesis is supported by the data for blowing at $\theta = 9.0$ deg (3 deg toward the outer wing panel), which is the worst case.

Variable SWB Rates

The effects of variable SWB rates on the longitudinal aerodynamic characteristics are shown in Fig. 8. The C_L data show that at low α, the jet-induced camber effect causes a relatively constant lift increment. In the moderate α-range, the lift slope curves increase with SWB rates as would be expected. At the higher angles, the loss of lift is less abrupt and $C_{L\max}$ is greater (and occurs at a higher α) as SWB rates increase.

Comparison of the ΔC_L data with those in Figs. 5 and 6 shows that different SWB rates do not significantly alter the trends. Aside from the magnitude differences, there is a slight increase in α at $\Delta C_{L\max}$ as SWB rates increase. Note that the payoff in lift effectiveness diminishes with increasing C_μ.

The effect of varying the SWB rate on longitudinal stability is presented in Fig. 8. Two main points with respect to the baseline can be made as SWB rates are increased: 1) stability levels were increased throughout the α-range, and 2) pitchup was delayed to higher α or was eliminated (namely, $C_\mu = 0.070$). It is remarkable that a blowing coefficient of 0.035, within the capabilities of the F-4C test-bed aircraft, was able to delay pitchup and increase the usable C_L from approximately 0.8 to 1.1.

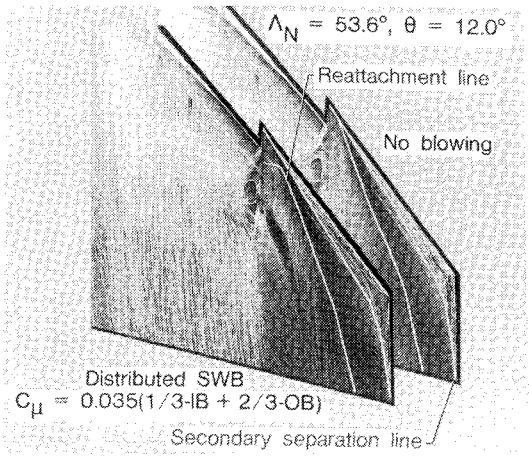

Fig. 6a Effect of SWB on wing upper surface; oil visualization at $\alpha = 6$ deg.

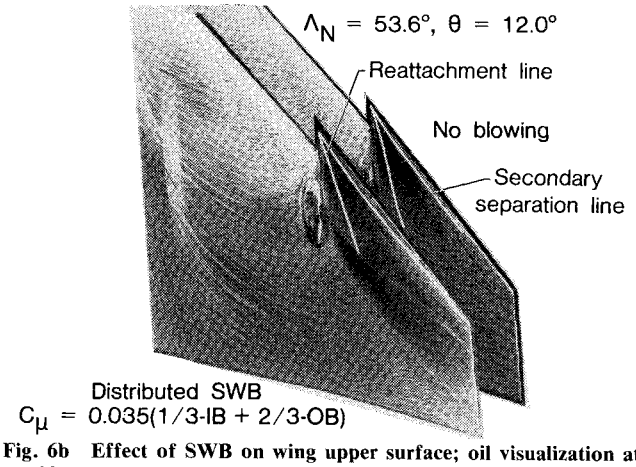

Fig. 6b Effect of SWB on wing upper surface; oil visualization at $\alpha = 20$ deg.

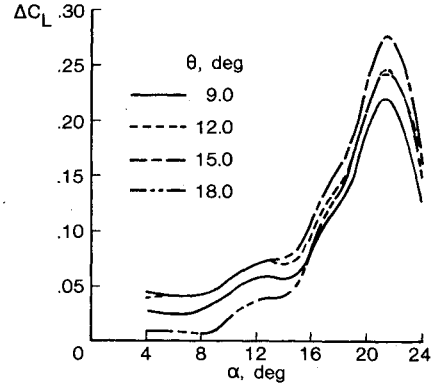

Fig. 7 Effects of outboard nozzle elevation angle on the incremental lift coefficient; clean configuration, ALL-OB, $C_\mu = 0.035$, $\Lambda_N = 53.6$ deg.

The ratio of C_L with blowing to C_L with no blowing ($C_L/C_{L_{C_\mu=0}}$) is a figure of merit that indicates the lift effectiveness of SWB. As shown at the top of Fig. 9, SWB effectiveness is nearly constant up to $\alpha \approx 16$ deg for all SWB rates, with greater levels occurring in the higher α-range. Also presented in Fig. 9 is the lift augmentation ratio ($\Delta C_L/C_\mu$), which is another indicator of the effectiveness of SWB to produce lift. This ratio highlights several interesting aspects of lift-producing jets. First, when $\Delta C_L/C_\mu < 1$, the blowing jet would be more effective when used for direct lift. (See the data for $C_\mu = 0.070$ at $\alpha < 10$ deg.) Second, the effectiveness of SWB to produce lift decreases as rates are increased, which Ref. 11 suggests is an indication that the lowest SWB rate is

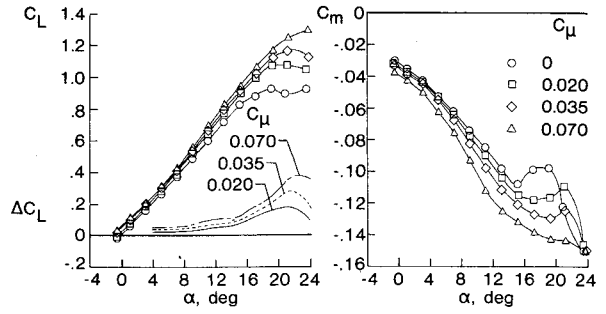

Fig. 8 Effects of variable SWB rates on the longitudinal aerodynamic characteristics; clean configuration, ALL-OB, $\Lambda_N = 53.6$ deg, $\theta = 15.0$ deg.

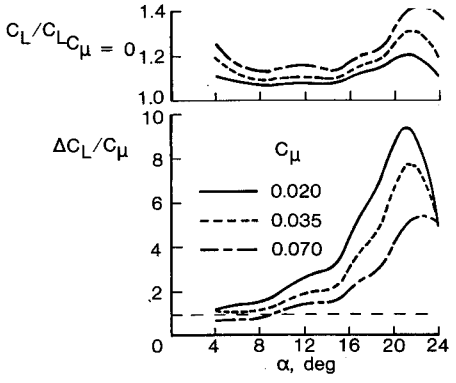

Fig. 9 Effects of variable SWB rates on SWB effectiveness and lift augmentation ratio; clean configuration, ALL-OB, $\Lambda_N = 53.6$ deg, $\theta = 15.0$ deg.

sufficient to stabilize the vortex, and higher rates only provide moderate enhancement.

Distributed Spanwise Blowing Studies

Clean Configuration

An unexpected result can be noted in the C_L and ΔC_L data (Fig. 10), where the blowing arrangements of ALL-IB, and 2/3-IB and 1/3-OB have less lift than the baseline up to $\alpha = 16$ and 12 deg, respectively. Beyond $\alpha = 16$ deg, the lift curves for these two cases continue to increase, indicating that $C_{L\max}$ should occur at an α higher than was tested. For blowing ALL-OB, and 1/3-IB and 2/3-OB, the results showed a small incremental lift improvement at low α, more nonlinear lift in the mid α-range, and further improvement at higher α.

The effects of distributed SWB on longitudinal stability are presented in Fig. 10. While all distributed blowing cases show approximately the same stability level, other differences can be noted. The pitching moment increments became more negative as the distribution is shifted outboard but, more importantly, the instability of the baseline is alleviated as the majority of blowing is shifted inboard. Note that at $\alpha > 20$ deg, the large, undesirable nose-down moment was reduced when the majority of SWB was distributed inboard.

The lateral-directional stability characteristics for distributed SWB are presented in Fig. 11. As the data show, SWB has minimal effect on lateral stability (C_{ℓ_β}) at low α. Between $\alpha \approx 10$ and 20 deg, stability levels decrease from the baseline as SWB is distributed from all outboard to all inboard. At higher α's, stability decreases as the majority of SWB is distributed outboard. In fact, instability occurred at a lower α than the baseline when the model was configured for ALL-OB, and 1/3-IB and 2/3-OB distributions. The directional stability (C_{n_β}) data show that SWB has little effect below $\alpha \approx 20$ deg that instability occurs for all SWB distributions in a narrow α-band ($\approx$22–25 deg), and that there is a slight advantage as SWB is distributed inboard.

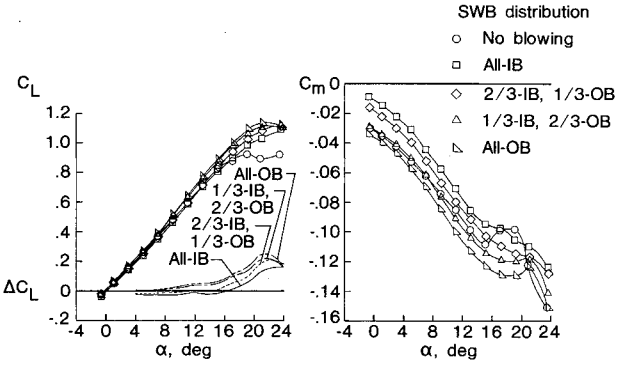

Fig. 10 Effects of distributed SWB on the longitudinal aerodynamic characteristics; clean configuration, $C_\mu = 0.035$, $\Lambda_N = 53.6$ deg, $\theta = 12.0$ deg.

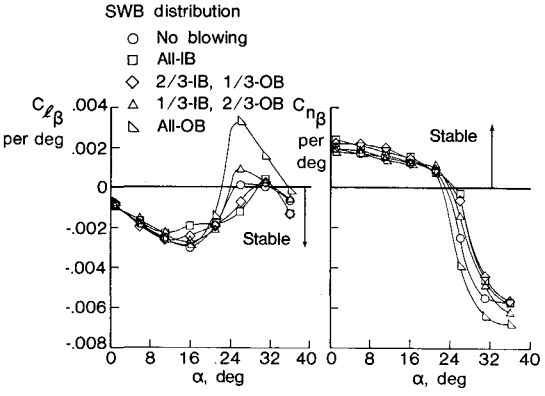

Fig. 11 Effects of distributed SWB on the lateral-directional stability characteristics; clean configuration, $C_T = 0.035$, $\Lambda_N = 53.6$ deg, $\theta = 12.0$ deg.

The parameter $C_{n_{\beta,\mathrm{dyn}}}$, which is a combination of the two static derivatives just discussed, is an indicator of resistance to the directional divergence (nose-slice) phenomenon of high-performance aircraft with the tendency to diverge occurring when $C_{n_{\beta,\mathrm{dyn}}} < 0$ (Ref. 12). As the data in Fig. 12 show, divergence resistance is reduced below that of the baseline for the ALL-OB distribution, whereas divergence resistance is increased when the majority of SWB is inboard, owing chiefly to the improvement in the effective dihedral parameter (C_{ℓ_β}).

The roll damping data (Fig. 12) defined as $C_{\ell_p} + C_{\ell_{\dot\beta}} \cdot \sin\alpha$, show that the baseline becomes lightly damped for $\alpha \approx$ 16-20 deg, indicating a susceptibility for an undamped oscillation such as wing rock. In this α-range the three SWB distributions show improved roll damping characteristics, which should reduce the severity of wing rock. Also note that at $\alpha \approx 26$ deg, blowing ALL-OB has approximately twice as much damping as the other distribution.

Results of tethered free-flight tests showed that the no blowing configuration exhibited good flying qualities through $\alpha = 20$ deg, although wing rock was only lightly damped. At $\alpha = 23$ deg, pilot work load increased due to reduced directional stability and roll damping. Directional divergence occurred at $\alpha = 28$ deg due to loss of directional stability, even though roll damping increased slightly. When SWB ($C_T = 0.035$) was distributed ALL-IB, good flying qualities were extended to $\alpha = 24$ deg. Some loss in control response was experienced at $\alpha = 26$ deg, but no increase in pilot work load was noted. Directional divergence was delayed until $\alpha = 32$ deg. For SWB ($C_T = 0.035$) distributed 1/3-IB and 2/3-OB, good flying qualities were maintained to $\alpha = 24$ deg except for a slight reduction in rudder authority. Directional divergence, however, occurred at $\alpha = 28$ deg (same as no blowing) due to loss of directional stability.

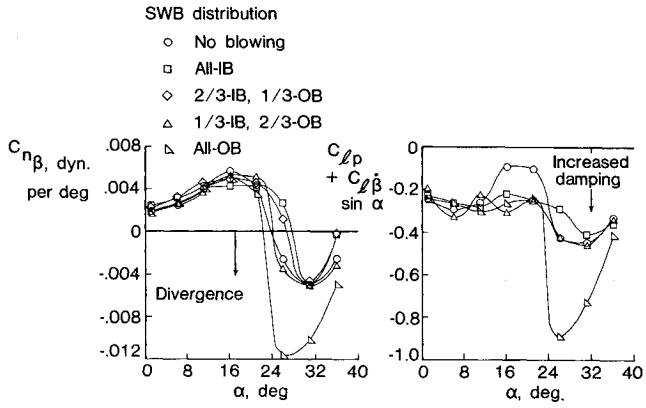

Fig. 12 Effects of distributed SWB on departure resistance and damping in roll parameter; clean configuration, $C_T = 0.035$, $\Lambda_N = 53.6$ deg, $\theta = 12.0$ deg.

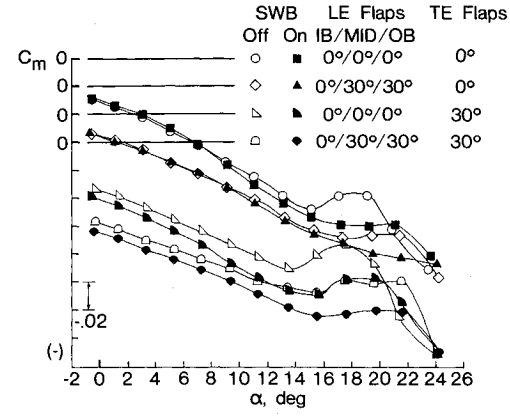

Fig. 14 Effects of distributed SWB on the pitching moment coefficient with leading- and trailing-edge flaps; $C_\mu = 0.035$, 1/3-IB, 2/3-OB, $\Lambda_N = 53.6$ deg, $\theta = 12.0$ deg.

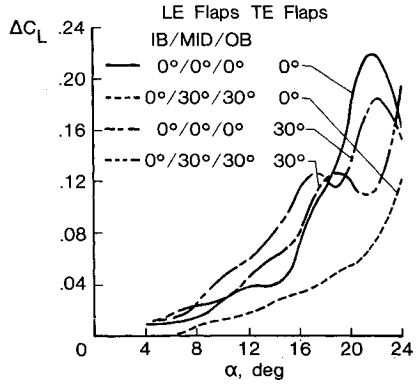

Fig. 13 Effects of distributed SWB on the incremental lift coefficient with leading- and trailing-edge flaps; $C_\mu = 0.035$, 1/3-IB, 2/3-OB, $\Lambda_N = 53.6$ deg, $\theta = 12.0$ deg.

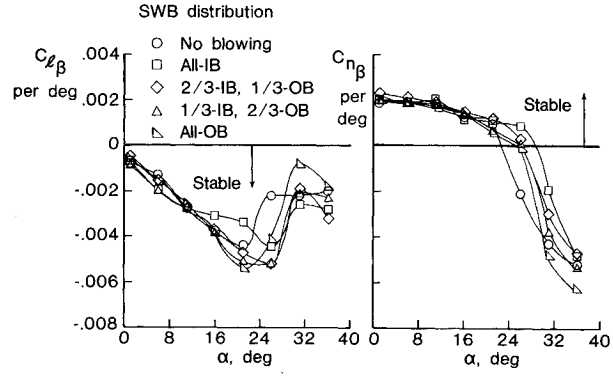

Fig. 15 Effects of distributed SWB on the lateral-directional stability characteristics with leading-edge flaps; IB, MID, OB LE Flaps at 0, 45, and 45 deg, respectively, $C_T = 0.035$, $\Lambda_N = 53.6$ deg, $\theta = 12.0$ deg.

Leading- and Trailing-Edge Flaps

Three configurations have been selected to show the effects of SWB on the performance of high lift devices. When deflected, the inboard, mid-, and outboard leading-edge (LE) flaps were at angles of 0, 30, and 30 deg, respectively, and the trailing-edge (TE) flaps were at 30 deg. The blowing coefficient of 0.035 as distributed 1/3-IB and 2/3-OB. Undeflected flap data have been included for comparison.

LE flap-only data (ΔC_L), presented in Fig. 13, show that SWB has only a marginal effect up to $\alpha \approx 22$ deg. As would be expected, LE camber delayed lift effectiveness and vortex formation to higher angles of attack. However, above 22 deg, the rather abrupt slope increase indicates that $\Delta C_{L\max}$ would occur at an α higher than the range of this test. Spanwise blowing improved the incremental lift effectiveness of TE flaps between $\alpha = 4$ and 18 deg. This would suggest that blowing 1/3-C_μ inboard well forward of the TE flaps is sufficient to reduce the development of the adverse pressure gradient associated with deflected TE flaps. Above 18 deg, the merging of the data with the undeflected flap baseline indicates the loss of TE flap effectiveness. The ΔC_L data, for a combination of LE and TE flaps, show the favorable effect of SWB between $\alpha \approx 12$ and 18 deg, which can be attributed to TE flap effectiveness. As was alluded to earlier, the improvement above $\alpha \approx 22$ deg can be attributed to LE vortices emanating from the flaps that are enhanced by SWB. Data from a similar test (0.10-scale F-5E model with inboard blowing and LE and TE flaps) showed $C_{L\max}$ occurred in the mid 30 deg α-range,[13] which supports the premise that distributed SWB would improve the lift effectiveness of a combination of LE and TE flaps above $\alpha = 24$ deg.

The pitching moment data for high lift devices with and without blowing are presented in Fig. 14. Undeflected flap data (baseline) are shown at the top for comparison. For no blowing, the main effect of LE flaps is to delay pitchup of the baseline ($\approx$ deg α). Remarkably, LE flaps with blowing have eliminated the instability and subsequent large pitchdown at higher α's. This favorable effect of SWB is probably due to the stabilization of the LE vortex on the outer wing panel whereas, without blowing, vortex breakdown occurs, moving the a.c. forward. TE flap-only data (no blowing) indicate pitchup at $\alpha \approx 13$ deg, which is delayed by only 2 deg with SWB. This can be attributed to separation on the TE flaps due to flap deflection. The last set of curves (LE and TE flaps) shows trends similar to those just discussed. It can be concluded that, while LE flaps with blowing had desirable longitudinal characteristics, deflected TE flaps caused separation of the flaps (alone or in combination with LE flap) and perhaps were overdeflected.

The lateral-directional stability characteristics for distributed SWB are presented in Fig. 15 for the configuration of inboard, mid, and outboard LE flaps down 0, 45, and 45 deg, respectively. Comparison of the data with those contained in Fig. 11 shows that LE flaps had a dramatic stabilizing effect on the lateral stability: note that the slope reversal has been extended by about 5 deg, that all distributions remained stable throughout the α-range of the test, and that SWB increased stability between $\alpha \approx 11$ and 28 deg, except for the ALL-IB distribution. The use of SWB with LE flaps also improved directional stability; e.g., directional instability was delayed ≈ 6 deg for the ALL-IB distribution. Test results on a similar configuration (Ref. 14, no SWB) indicated that the loss

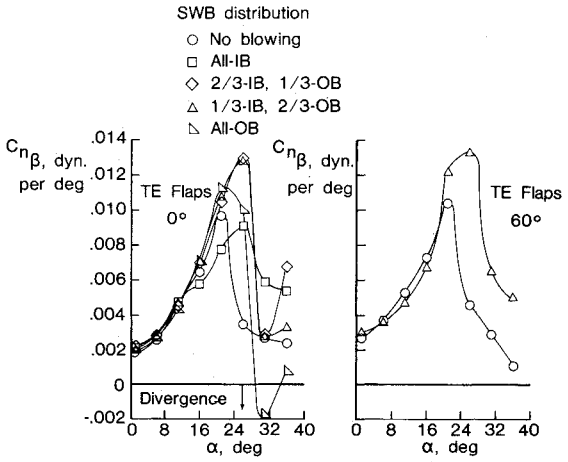

Fig. 16 Effects of distributed SWB on departure resistance with leading- and trailing-edge flaps; IB, MID, OB LE flaps at 0, 45, and 45 deg, respectively, $C_T = 0.035$, $\Lambda_N = 53.6$ deg, $\theta = 12.0$ deg.

of directional stability was caused by vertical tail encountering both an adverse sidewash flowfield and the stalled wake of the wing.

The effects of distributed SWB on the directional divergence parameter ($C_{\eta\beta,\mathrm{dyn}}$) for two flap configurations are presented in Fig. 16. LE flap-only data (at the left) show that with SWB, departure resistance was comparable to, or better, than the baseline, except for the ALL-OB distribution. With TE flaps down, the limited data at the right indicate similar trends.

With the TE flaps up and the inboard, mid, and outboard LE flaps down 0, 60, and 60 deg, respectively, tethered free-flight tests indicated that, for no blowing, good flying qualities were experienced to $\alpha = 24$ deg which was the α for onset of wing rock. Directional divergence occurred at $\alpha = 27$ deg. Distributing SWB ($C_T = 0.035$) all inboard provided good flying qualities at $\alpha = 27$ deg, even with a slight loss of roll damping. There was a minor reduction in control response accompanied by light wing rock between $\alpha = 32$ and 34 deg, which was followed by directional divergence at $\alpha = 35$ deg. When SWB ($C_T = 0.035$) was distributed 1/3-IB and 2/3-OB, good flying qualities were maintained to $\alpha = 28$ deg. However, wing rock increased in severity just prior to directional divergence ($\alpha = 35$ deg). Good flying qualities were sustained to $\alpha = 23$ deg with SWB ($C_T = 0.035$) distributed all outboard. At $\alpha = 28$ deg, a loss of roll damping was noted, followed by a loss of directional stability ($\alpha = 32$ deg) and eventually directional divergence at $\alpha = 34$ deg.

Concluding Remarks

Results of these wind-tunnel experiments on scale F-4C models showed that blowing a jet of air of reasonable strength spanwise on the outer panels of a moderately swept wing improved both lift effectiveness and longitudinal stability. Through the mechanism of flow entrainment, these jets stabilized and enhanced the leading-edge vortices, thus increasing nonlinear lift and delaying wing stall and vortex breakdown to much higher lift coefficients and angles of attack. These favorable characteristics were further improved as blowing rates increased. A near-optimum alignment for the outer panel nozzles was parallel to the leading edge and 3 deg above the wing. Distributing more blowing outboard increased lift and pitching moment levels; however, with the majority of blowing inboard, pitchup instability was eliminated. Spanwise blowing had a slightly degrading effect on the lateral-directional stability characteristics below ≈20 deg angle of attack but, above 20 deg, instabilities were delayed to higher angles as more blowing was distributed inboard. Results of tethered free-flight tests indicated that spanwise blowing delayed directional divergence to higher angles of attack and alleviated wing rock by providing increased roll damping.

Spanwise blowing improved the lift effectiveness and delayed longitudinal instability caused by trailing-edge flaps. With leading-edge flaps only, blowing eliminated pitchup and subsequent severe pitchdown, vastly improved lateral-directional stability characteristics, and enhanced lift effectiveness, although not to the levels experienced by the TE flap configurations.

Further, these tests on an F-4C scale model have substantiated lift enhancement due to jet/vortex interaction; however, the sensitivity of the stability characteristics to spanwise blowing distributions and rates requires thorough evaluation of each configuration. The use of spanwise blowing on current fighter aircraft is probably not feasible but does offer some interesting possibilities for the next-generation fighter (NGF). Spanwise blowing would improve the maneuver performance of the supersonically designed slender wing. In addition, if the NGF uses the leading-edge vortex flap to alleviate high drag due to leading-edge flow separation, then the blowing jet could be expected to trap the vortex on the flap and to further its effectiveness.

References

[1]Dixon, C.J., Theisen, J.G., and Scruggs, R.M., "Theoretical and Experimental Investigations of Vortex Lift Control by Spanwise Blowing," *Experimental Research* (Vol. I) and *Three-Dimensional Theory for Vortex-Lift Augmentation* (Vol. II) LG73ER-0169, Sept. 1973.

[2]Bradley, R.G., Wray, W.O., and Smith, C.W., "An Experimental Investigation of Leading-Edge Vortex Augmentation by Blowing," NASA CR-132415, April 1974.

[3]Campbell, J.F., "Effects of Spanwise Blowing on the Pressure Field and Vortex-Lift Characteristics of a 44° Swept Trapezoidal Wing," NASA TN D-7907, 1975.

[4]Erickson, G.E. and Campbell, J.F., "Improvement of Maneuver Aerodynamics by Spanwise Blowing," NASA TP-1065, Dec. 1977.

[5]Rousseau, W.A., et al. "Model F-4C Performance Characteristics With Spanwise Blowing," McDonnell Aircraft Company, MDC A6289, Dec. 1979.

[6]Dixon, C.J., Dansby, T., and Poisson-Quinton, P., "Benefits of Spanwise Blowing at Transonic Speeds," XI ICAS Congress, ICAS Paper A1-01, Lisbon, Sept. 1978.

[7]Fox, C.H. Jr. and Huffman, J.K., "Calibration and Test Capabilities of the Langley 7- by 10-Foot High Speed Tunnel," NASA TM X-74027, May 1977.

[8]Grafton, S.B. and Libbey, C.E., "Dynamic Stability Derivatives of a Twin-Jet Fighter Model for Angles of Attack from −10° to 110°," NASA TN D-6091, 1971.

[9]Chambers, J.R., Bowman, J.S. Jr., and Malcom, G.N., "Stall/Spin Test Techniques Used by NASA," AGARD CP-199, June 1976.

[10]Dixon, C.J., "Lift Augmentation by Lateral Blowing Over a Lifting Surface," AIAA Paper 69-193, Feb. 1969.

[11]Anglin, E.L. and Satran, D., "Effects of Spanwise Blowing on Two Fighter Airplane Configurations," *Journal of Aircraft,* Vol. 17, Dec. 1980.

[12]Greer, H.D., "Summary of Directional Divergence Characteristics of Several High-Performance Aircraft Configurations," NASA TN D-6993, Nov. 1972.

[13]Erickson, G. E., "Effect of Spanwise Blowing on the Aerodynamic Characteristics of the F-5E, AIAA Paper 79-0118, Oct. 1979.

[14]Chambers, J. R. and Anglin, E. L., "Analysis of Lateral-Directional Stability Characteristics of a Twin-Jet Fighter Airplane at High Angles of Attack, NASA TN D-5361, Aug. 1969.